Vanadia−Silica Low-Temperature Aerogels: Influence of Aging and Vanadia Loading on Structural and Chemical Properties

D. C. M. Dutoit, M. Schneider,† P. Fabrizioli, and A. Baiker*

Department of Chemical Engineering and Industrial Chemistry, Swiss Federal Institute of Technology, ETH-Zentrum, CH-8092 Zürich, Switzerland

Received September 13, 1995. Revised Manuscript Received December 15, 1995⊗

Vanadia−silica mixed oxides were prepared via the sol−gel method involving acid catalysis together with prehydrolysis in order to achieve matching of the reactivities of vanadium(V) oxide triisopropoxide and tetraethoxysilicon(IV) precursors. Gelation was forced by the addition of basic solution. The as-received gels were supercritically dried by semicontinuous extraction with supercritical CO_2 at 313 K (low-temperature aerogels). The effects of composition, aging, and calcination temperature on the chemical, structural, and textural properties of the solids were investigated. The oxides were characterized by N_2 physisorption, XRD, vibrational spectroscopy, thermal analysis, UV−vis, and ^{51}V NMR. The low-temperature vanadia−silica aerogels were mesoporous and highly disperse. The increasing V content from 5 to 20 wt % nominal V_2O_5 caused a gradual decline in V dispersion. For 30 wt % "V_2O_5" the continuous formation of V−O−V connectivity resulted in crystallization of V_2O_5. The effect of aging in basic medium confined to the textural properties, significantly increasing BET surface area and especially pore volume. The prepared aerogels revealed a marked lack of stability against both apolar solvents in the presence of peroxides and polar solvents. The marked thermal stability in air at ≤873 K, however, combined with mesoporosity and high V dispersion, render these solids promising catalysts for gas-phase reactions.

Introduction

The excellent activities in the epoxidation of bulky olefins by the use of titania−silica low-temperature aerogels[1,2] prompted us to extend our studies to other silica-based mixed oxides. Silica-supported vanadia,[3−7] vanadia−silica xerogels,[8−10] and vanadium-containing silicalites (VS-1, VS-2)[11−16] have been shown to possess interesting catalytic properties for the selective catalytic reduction of NO with NH_3,[8,14] selective oxidation,[9,14,16] ammoxidation,[14,15] sulfoxidation,[16] conversion of methanol to hydrocarbons,[14] and oxidative dehydrogenation.[14]

Compared to silica-supported vanadia, vanadia−silica xerogels,[8] and especially V−silicalites[14] seem to possess different and/or in some cases superior catalytic performance. With V−silicalite, the catalytic prospect is likely to reside in atomically dispersed, reducible V^{5+} species that adopt a nearly symmetrical tetrahedral environment and are anchored to defect sites of the silicalite framework, probably as framework satellites.[11] However, vanadium-containing silicalites suffer from some severe limitations. First, the synthesis of pure, homogeneous, and well-characterizable V−silicalite has proved to be difficult, which mainly resides in alkali contamination, extraframework V_2O_5, polynuclear vanadium oxide, and nearly octahedral VO^{2+} species, and a rather low amount of stabilizable tetrahedral V^{5+}. Second, the small pores restrict the access to the internal surface by large organic reactants and thus impede the use for fine chemical synthesis.

Possible ways to overcome these limitations are either the formation of adequate silica supports followed by the selective immobilization of the vanadia precursor[5,6,17] or the introduction of both components in a single step by means of controlled solution−sol−gel (SSG) chemistry.[8] The former concept has been shown to lead to weak vanadia−support interactions, which is mirrored in the ease of hydrolysis and alcoholysis of

† Present address: F. Hoffmann-La Roche Ltd., VFH, CH-4070 Basel, Switzerland.

* To whom correspondence should be addressed.

⊗ Abstract published in *Advance ACS Abstracts,* February 1, 1996.

(1) Dutoit, D. C. M.; Schneider, M.; Baiker, A. *J. Catal.* **1995**, *153*, 165.
(2) Hutter, R.; Mallat, T.; Baiker, A. *J. Catal.* **1995**, *153*, 177.
(3) Bond, G. C.; Tahir, S. F. *Appl. Catal.* **1991**, *71*, 1.
(4) Gellings, P. J. *Catalysis* **1985**, *7*, 105.
(5) Baiker, A.; Dollenmeier, P.; Glinski, M.; Reller, A. *Appl. Catal.* **1987**, *35*, 351.
(6) Vogt, E. T. C.; de Boer, M.; van Dillen, A. J.; Geus, J. W. *Appl. Catal.* **1988**, *40*, 255.
(7) Centi, G.; Trifiro, F.; Ebner, J. R.; Franchetti, V. *Chem. Rev.* **1989**, *28*, 400.
(8) Baiker, A.; Dollenmeier, P.; Glinski, M.; Reller, A.; Sharma, V. K. *J. Catal.* **1988**, *111*, 273.
(9) Neumann, R.; Chava, M.; Levin, M. *J. Chem. Soc., Chem. Commun.* **1993**, 1685.
(10) Stiegman, A. E.; Eckert, H.; Plett, G.; Kim, S. S.; Anderson, M.; Yavrouian, A. *Chem. Mater.* **1993**, *5*, 1591.
(11) Bellussi, G.; Rigutto, M. S. *Advanced Zeolite Science and Applications, Studies in Surface Science and Catalysis*; Jansen, J. C., Stöcker, M., Karge, H. G., Weitkamp, J., Eds.; Elsevier Science B. V.: Amsterdam, 1994; Vol. 85, p 177.
(12) Miyamoto, A.; Medhanavyn, D.; Inui, T. *Chem. Expr.* **1986**, *1*, 559.
(13) Reddy, J. S.; Kumar, R.; Ratnasamy, P. *Appl. Catal.* **1990**, *58*, L1.
(14) Centi, G.; Perathoner, S.; Trifiro, F.; Aboukais, A.; Aissi, C. F.; Guelton, M. *J. Phys. Chem.* **1992**, *96*, 2617 and references therein.
(15) Sudhakar Reddy, J.; Sayari, A. *Catal. Lett.* **1994**, *28*, 263.
(16) Ramaswamy, A. V.; Sivasanker, S. *Catal. Lett.* **1993**, *22*, 239.
(17) Jehng, J.-M.; Wachs, I. E. *Catal. Lett.* **1992**, *13*, 9.

0897-4756/96/2808-0734$12.00/0

V−O−Si bonds and the low resistance toward thermally induced agglomeration−crystallization.[18] The one-step SSG preparation of vanadia−silica xerogels via mixing of preformed sols, however, was able to stabilize well-dispersed vanadia lamellae up to 873 K by their uniform distribution in the silica matrix. In general, the highly controllable SSG technique based on chiefly metal alkoxides[19,20] is a versatile and potent means for the synthesis of intimately mixed oxides and the control of their structure and composition at a molecular scale.[19,21,22] The inherent advantages comprise the use of a variety of wet-chemical preparation tailoring tools, purity of the precursors, molecular-scale mixing of the constituents, homogeneity of the SSG product, and ability to impose kinetic constraints and to stabilize metastable phase(s).

In particular, the preparation of intimately mixed oxides with interesting structural and chemical properties require evenly matched precursor reactivities. This matching is achieved and preserved by the following concepts, either by themselves or in combination with each other: (i) chemical modification of the more reactive precursor,[1,23,24] (ii) nature of the precursor,[1,23,24] (iii) prehydrolysis of the less reactive precursor,[1,23−26] (iv) use of inorganic acids to decouple hydrolysis and condensation (fast hydrolysis relative to condensation),[23,27] (v) different sol−gel temperature,[24] and (vi) different drying conditions.[1,28,29] Estimates of the SSG reactivity are derived from the so-called partial charge model[27] which is based on the principle of electronegativity equalization.[30] Since the metal centers of transition-metal alkoxides possess much higher positive partial charges as well as electronegativity than silicon in corresponding alkoxy compounds and furthermore exert the ability to increase their coordination number to values above the appropriate oxidation state, hydrolysis and condensation rates are generally much faster for transition-metal alkoxides than those for corresponding silicon alkoxides.[27] Last but not least, the structure and composition of the wet SSG product at molecular scale must be preserved during drying without drastic deterioration of the molecular-scale and textural characteristics.[22,31] These requirements may be accomplished by the use of low-temperature supercritical drying via semicontinuous extraction of the solvent with supercritical CO_2 (T_c = 304 K), leading to low-temperature aerogels.[22] Consequently, the coupling of the SSG process with subsequent supercritical drying offers a combination of the intrinsic advantages of the SSG method with the "structure- and texture-preserving" properties of low-temperature SCD.

With regard to physicochemical characterization, recently, new insights into the structural features at atomical scale of vanadia−silica xerogels have been provided by Stiegman et al.[32] They prepared a hybrid xerogel that contained discrete units of vanadium oxide throughout the glass. The transparency accounted for unique opportunity to obtain well-defined absorption, emission, and Raman spectra of the vanadium oxide species. In contrast to many previous studies which placed the highest occupied molecular orbital (HOMO) at the terminal V═O group, the HOMO is actually a nonbonding orbital localized on the basal plane ligands.

In conclusion, the interesting catalytic properties of atomically dispersed vanadium in V−silicalites with prevailing microporosity spurred us to prepare vanadia−silica mixed oxides with high V dispersion and meso- to macroporosity suitable for catalytic oxidation in both liquid and gas phase without any pore-size limitation. To our knowledge the effects of composition, aging, and calcination temperature, systematically varied over a wide range, on the structural and textural properties of low-temperature vanadia−silica aerogels have not been reported so far. Here, we demonstrate the catalytically prospected synthesis of vanadia−silica mixed oxides via fine tuning of sol−gel reactivity followed by structure "preserving" low-temperature supercritical drying.

Experimental Section

Sample Preparation. Throughout this work a set of acronyms is used, taking 10V*LT* as an example. The first numeral displays the designed content of nominal V_2O_5 in weight percent, based on the theoretical system V_2O_5−SiO_2 (5 wt % "V_2O_5" → 3.3 at. % V; 10 wt % → 6.8 at. %; 20 wt % → 14.2 at. %; 30 wt % → 22.1 at. %); V stands for vanadia−silica; the subsequent two capital letters represent the drying method used (*L*ow-*T*emperature supercritical drying).

Sol−Gel Preparation. The quantities and conditions of the appropriate sol−gel preparations are listed in Table 1. In general, the sol−gel process was carried out in an anti-adhesive, closed Teflon beaker (inner diameter 0.1 m), under nitrogen atmosphere, at ambient temperature (297 ± 2 K), and with a magnetic Teflon bead of 5 cm length. The total volume of the SSG sample was ca. 140 mL and the corresponding molar ratios n_{H_2O}:$n_{alkoxide}$:n_{acid} were 2:1:0.01.

The first solution consisted of 47.42 g of tetraethoxysilicon(IV) (TEOS; Fluka, purum) dissolved in 60 mL of ethanol (EtOH; Fluka, puriss, p.a.) and the second one (hydrolysant) of hydrochloric acid (HCl 37 wt %; Fluka, puriss, p.a.) and doubly distilled water. After homogenization of both solutions for 5 min, under vigorous stirring (1000 rpm) the hydrolysant was added to the TEOS solution via the dropping funnel for 1 min, and heated to 323 K for 90 min (prehydrolysis of TEOS). After cooling the solution to ambient temperature, the vanadium(V) oxide triisoproposide (VOTIP; Gelest) in 8 mL of EtOH (orange-brown solution) was introduced under vigorous stirring. The as-received sol was aged for 60 min at 323 K and 14 h at ambient temperature. The gelation was forced by ammonium hydroxide (NH_4OH; Fluka, puriss, p.a.) diluted in EtOH (V_{EtOH}:V_{NH_4OH} = 6:1). First, 12 mL of the basic solution was added dropwise for 1 min; afterward another 6 mL was

(18) Schraml-Marth, M.; Wokaun, A.; Pohl, M.; Krauss, H.-L. *J. Chem. Soc., Faraday Trans.* **1991**, *87*, 2635.
(19) Brinker, C. J.; Scherer, G. W. *Sol−Gel Science−The Physics and Chemistry of Sol−Gel Processing*; Academic Press: San Diego, 1990.
(20) Bradley, D. C.; Mehrotra, R. C.; Gaur, D. P. *Metal Alkoxides*; Academic Press: London, 1978.
(21) Ward, D. A.; Ko, E. I. *Ind. Eng. Chem. Res.* **1995**, *34*, 421.
(22) Schneider, M.; Baiker, A. *Catal. Rev.−Sci. Eng.* **1995**, *37*, 515.
(23) Aizawa, M.; Nosaka, Y.; Fujii, N. *J. Non-Cryst. Solids* **1991**, *128*, 77.
(24) Miller, J. B.; Rankin, S. E.; Ko, E. I. *J. Non-Cryst. Solids* **1994**, *148*, 673.
(25) Yoldas, B. E. *J. Non-Cryst. Solids* **1980**, *38*, 81.
(26) Miller, J. B.; Johnston, S. T.; Ko, E. I. *J. Catal.* **1994**, *150*, 311.
(27) Livage, J.; Henry, M.; Sanchez, C. *Prog. Solid State Chem.* **1988**, *18*, 259.
(28) Cogliati, G.; Guglielmi, M.; Che, T. M.; Clark, T. J. *Mater. Res. Soc. Symp. Proc.* **1990**, *180*, 329.
(29) Beghi, M.; Chiurlo, P.; Costa, L.; Palladino, M.; Pirini, M. F. *J. Non-Cryst. Solids* **1992**, *145*, 175.
(30) Sanderson, R. T. An Interpretation of Bond Lengths and a Classification of Bonds. *Science* **1951**, *114*, 670.
(31) Scherer, G. W. *J. Am. Ceram. Soc.* **1990**, *73*, 3.
(32) Tran, K.; Hanning-Lee, M. A.; Biswas, A.; Stiegmann, A. E.; Scott, G. W. *J. Am. Chem. Soc.* **1995**, *117*, 2618.

Table 1. Quantities, Composition, and Aging Times of the Sol−Gel Preparations[a]

samples	VOTIP[b] [mmol]	TEOS[c] [mmol]	37wt % HCl [mmol]	H_2O [mmol]	1. aging period[d] [h]	NH_4OH in EtOH[e] [mL]	2. aging period[f] [cycles]	3. aging period[g] [days]
0V*LT*		228	2.3	456	15	12	0	0
5V*LT*	7.9	228	2.4	472	15	12	0	0
4V*LT*a	7.9	228	2.4	472	15	12	0	16
10V*LT*	16.7	228	2.5	490	15	12	1	0
20V*LT*	37.6	228	2.7	531	15	12	2	0
30V*LT*	64.6	228	2.9	585	15	12	3	0

[a] Designations of the samples are explained in the Experimental Section. [b] Vanadium(V) oxide triisopropoxide (VOTIP). [c] Tetraethoxysilicon(IV) (TEOS). [d] Reduced stirring (ca. 500 ppm), 1 h at 323 K and 14 h at ambient temperature. [e] Ammonium hydroxide (NH_4OH) in ethanol (EtOH) (V_{EtOH}:V_{NH_4OH} = 6:1). [f] One cycle contained aging over 30 min under reduced stirring at ambient temperature and adding 6 mL of the basic mixture[e] over 1 min. The cycles were repeated until gelation occurred. [g] Aging hermetically closed at ambient temperature.

introduced every 30 min until gelation occurred. With 5V*LT*a, the wet-chemical preparation of the gel corresponded to that for 5V*LT*; after gelation, however, 5V*LT*a was additionally aged for 16 days at ambient temperature. The higher the vanadia content, the more base was needed. The colors of the gels with 5, 10, 20, and 30 wt % nominal V_2O_5 were light-yellow, yellow, green, and brown, respectively.

Drying of the Gels. Semicontinuous extraction of the solvent with supercritical CO_2 was performed to produce low-temperature aerogels. To suppress flushing out of the wet-chemical SSG product, only gels were transferred into an autoclave with a net volume of 2 dm^3. The sample was stirred by a turbine stirrer (ca. 60 rpm) to minimize temperature inhomogeneities during the whole extraction procedure and bypassing of the gel lumps. Within 1 h and at a temperature of 313 K, the autoclave was pressurized with supercritical CO_2 to 24 MPa and the liquid−gas separator to 1 MPa, which resulted in an overall amount of 2.3 kg of CO_2. The solvent of the SSG product was semicontinuously extracted by a CO_2 flow of 20 g min^{-1} for 5 h (6 kg of CO_2) at a temperature of 313 K. The pressure was then isothermally released at ca. 20 g min^{-1}. Finally, the system was allowed to cool to ambient temperature. The resulting lumpy product was ground in a mortar. The colors of the produced aerogels with 5, 10, 20, and 30 wt % nominal V_2O_5 were white, reddish, and greenish, respectively.

Calcination Procedure. Portions of the uncalcined (raw) aerogel powder were calcined in a tubular reactor with upward flow. The temperature given corresponded to the oven temperature. The sample amount was ca. 2 g in all cases. To remove most of the organic residues prior to calcination, all aerogel samples were first pretreated in a nitrogen flow of 0.5 dm^3 min^{-1} for 1 h. They were heated at 5 K min^{-1} to 673 K. After being cooled to ca. 353 K, they were heated again at 5 K min^{-1} in air flowing at 0.5 dm^3 min^{-1} and held for 5 h at 673 or 873 K.

Composition Analysis. The composition was generally calculated based on the designed amounts used and independently confirmed by X-ray fluorescence spectroscopy (XRFS) analysis.

Physicochemical Characterization. *Nitrogen Physisorption.* The specific surface areas (S_{BET}), mean cylindrical pore diameters ($\langle d_p \rangle$), and specific desorption pore volumes ($V_{p(N_2)}$) were determined by nitrogen physisorption at 77 K using a Micromeritics ASAP 2000 instrument. Note that ($V_{p(N_2)}$) was assessed by the Barrett−Joyner−Halenda (BJH) method,[33] which is assumed to cover the cumulative desorption pore volume of pores in the maximum range 1.7−300 nm diameter. Prior to measurement, the samples calcined at 673 or 873 K were degassed for 5 h at 473 K. The raw samples were degassed at 353 K for 16 h. The final pressure was ca. 0.1 Pa in the closed system for at least 1 min. BET surface areas were calculated in a relative pressure range between 0.05 and 0.2 assuming a cross-sectional area of 0.162 nm^2 for the nitrogen molecule. The pore size distributions were calculated applying the BJH method[33] to the desorption branches of the isotherms.[34] The assessments of microporosity (V_t, S_t) were made from *t*-plot constructions in the range $0.3 < t < 0.5$ nm, using the Harkins−Jura correlation.[35]

X-ray Diffraction. X-ray powder diffraction (XRD) patterns were measured on a Siemens θ/θ D5000 powder X-ray diffractometer. The diffractograms were recorded with Cu Kα radiation over a 2θ range of 13−60° or 13−35° in the case of poorly crystalline samples. The detector used was a scintillation counter with secondary monochromator.

FTIR Spectroscopy. FTIR measurements were performed on a Perkin-Elmer Series 2000 NIR FT Raman instrument. The self-supporting sample wafers consisted of 100 mg of dry KBr and ca. 1 mg of sample; they were dehydrated in situ by heating to 403 K for 1 h. The sample cell was purged with a small flow of oxygen during the measurements. 500 scans were accumulated for each spectrum in transmission, at a spectral resolution of 4 cm^{-1}. The spectrum of dry KBr was taken for background subtraction.

By analogy with titania−silica,[1] the FTIR spectra of vanadia−silica mixed oxides are characterized by a generic band which can be attributed to an asymmetric stretching mode of SiO_4 tetrahedrons connected to V ions. This band was found at ca. 960 cm^{-1} for V-silicalites[11,36−38] and at about 950 cm^{-1} for vanadia−silica xerogels.[9] As regards our studies on titania−silica[1] this band proved to be a pertinent tool for the semiquantitative estimate of the Si−O−Ti connectivity. With unitary silica xerogels, the peak at 980 cm^{-1} was assigned to Si−OH vibrations.[39] Thus silanol vibrations are likely to superimpose on the Si−O−V stretching modes.

For the evaluation of the FTIR results four bands were deconvoluted into Gauss curves. The positions and corresponding assignments of these vibrations are surveyed as follows: (i) 800 cm^{-1},[19,40] 810 cm^{-1} [39] for symmetric ν(Si−O−Si) stretching vibration; (ii) 950−960 cm^{-1} assumed for ν(Si−O−V) vibration[9,11,36−38] and 980 cm^{-1} for Si−OH vibrations;[39] (iii) 1080 cm^{-1},[19] 1095 cm^{-1},[39] 1080−1105 cm^{-1} [40] for asymmetric ν(Si−O−Si) stretching vibration; (iv) 1180 cm^{-1},[39] 1200 cm^{-1},[40] 1220 cm^{-1},[19] for asymmetric ν(Si−O−Si) stretching vibration.

For the deconvolution the starting values were chosen at 800, 950, 1080, and 1220 cm^{-1}. The deconvoluted band positions of the calcined silica and vanadia−silica aerogels were in the range 779−810, 928−937, 1071−1085, and 1206−1220 cm^{-1}. To suppress any deterioration of the Si−O−V analysis, the deconvoluted Si−OH peak area of the calcined silica aerogel at 937 cm^{-1} was deducted from the corresponding peak areas of the binary aerogels, that is, proportionally to the appropriate SiO_2 content in atom percent.

(33) Barrett, E. P.; Joyner, L. G.; Halenda, P. P. *J. Am. Chem. Soc.* **1951**, *73*, 373.

(34) Broekoff, J. C. P. *Preparation of Heterogeneous Catalyst II*; Delmon, B., Grange, P., Jacobs, P., Poncelet, G., Eds.; Elsevier: Amsterdam, 1979; p 663.

(35) Harkins, W. D.; Jura, G. *J. Chem. Phys.* **1943**, *11*, 431.

(36) Hari Prasad Rao, P. R.; Kumar, R.; Ramaswamy, A. V.; Ratnasamy, P. *Zeolites* **1993**, *13*, 663.

(37) Hari Prasad Rao, P. R.; Ramaswamy, A. V.; Ratnasamy, P. *J. Catal.* **1992**, *137*, 225.

(38) Tuel, A.; Ben Taarit, Y. *Appl. Catal. A: General* **1993**, *102*, 201.

(39) Schraml-Marth, M.; Walther, K. L.; Wokaun, A.; Handy, B. E.; Baiker, A. *J. Non-Cryst. Solids* **1992**, *143*, 93.

(40) Duran, A.; Serna, C.; Fornes, V.; Fernandez-Navarro, J. M. *J. Non-Cryst. Solids* **1986**, *82*, 69.

Table 2. Textural Properties and Carbon Contents of the Vanadia−Silica Aerogel Samples Calcined in Flowing Air and Their Uncalcined Parent Aerogels[a]

sample	calc (K)	S_{BET} (S_t) (m^2/g)[b]	$V_{p(N_2)}$ (V_t) (cm^3/g)[c]	$\langle d_p \rangle$ (nm)[d]	C content (%)[e]
0V*LT*	673	981(167)	1.9(0.1)	8(20)	0.5(10.3)
	873	892(67)	1.8(0.0)	8(19)	0.2(10.3)
5V*LT*		705(0)	1.2(0.0)	7(11)	(9.9)
	673	888(131)	1.4(0.1)	6(12)	1.3(9.9)
	873	995(96)	1.6(0.0)	6(11)	0.1(9.9)
5V*LT*a		922(0)	2.7(0.0)	12(19)	(11.2)
	673	1108(55)	2.8(0.0)	10(19)	0.7(11.2)
	873	989(0)	2.5(0.0)	10(19)	0.2(11.2)
10V*LT*	673	840(53)	1.8(0.0)	9(17)	0.9(6.4)
	873	728(37)	1.7(0.0)	9(15)	0.2(6.4)
20V*LT*	673	597(48)	1.9(0.0)	13(32)	0.5(3.0)
	873	424(0.0)	1.7(0.0)	16(27)	0.1(3.0)
	1173	8(5)	≪0.1(0.0)	10(30)	0.1
30V*LT*	673	432(39)	0.7(0.0)	7(8)	0.4(21.5)
	873	167(1)	0.6(0.0)	14(21)	0.1(21.5)

[a] Designations of the samples are explained in the Experimental Section. [b] (S_t), in parentheses, denotes specific micropore surface area derived from *t*-plot analysis. [c] $V_{p(N_2)}$ designates the BJH cumulative desorption pore volume of pores in the maximum range 1.7−300 nm diameter; (V_t), in parentheses, denotes specific micropore volume derived from *t*-plot analysis. [d] $\langle d_p \rangle = 4V_{p(N_2)}/S_{BET}$; in parentheses, the graphically assessed pore size maximum of the pore size distribution derived from the desorption branch are given. [e] Carbon contents derived from elemental microanalysis; in parentheses, C content of the raw parent aerogels.

On the basis of this finding, eq 1 has been derived for forming an estimate of Si−O−V connectivity (V dispersion), *D*(Si−O−V):

$$D(\text{Si}-\text{O}-\text{V}) = \frac{S(\text{Si}-\text{O}-\text{V})}{S(\text{Si}-\text{O}-\text{Si})} \frac{x_{Si}}{x_V} \quad (1)$$

S(Si−O−V) and *S*(Si−O−Si) are the deconvoluted peak areas of the ν(Si−O−V) band at 928−937 cm^{-1} and the ν(Si−O−Si) band at 1206−1220 cm^{-1}; x_{Si} and x_V designate the molar proportions of Si and V, respectively. *D*(Si−O−V) values are assumed to reflect a semiquantitative measure of the proportion of Si−O−V species related to the overall V content and thus a kind of mixing efficiency or estimate of V dispersion. The standard deviation of the *D*(Si−O−V) analysis is ca. 3%, as determined in ref 1. As concerns the raw aerogels, the large amounts of remnant organic residues caused considerable backgrounds, which impeded reliable analysis of vibration spectroscopy. The carbon contents of the uncalcined samples determined by elemental microanalysis ranged up to 11.2 wt % (Table 2).

FT Raman spectroscopy. For the Raman measurements the samples were introduced in a metallic sample holder with a 4 mm drilling. Spectra were excited using the 1033 nm line of a YAG laser (Spectron Laser Systems). The backscattered light was analyzed by a Perkin-Elmer Series 2000 NIR FTRaman instrument. To the binary aerogel with 30 wt % nominal V_2O_5 and unitary V_2O_5 (Fluka, purum) 0.9 W of laser power were focused on the samples, whereas for the other aerogels 0.1 W were used. Prior to measurement, the samples were dehydrated in situ by heating at the appropriate laser power for 30 min, resulting in ca. 350 and 550 K at 0.1 and 0.9 W of laser power, respectively. 512 scans were accumulated for each spectrum, at a spectral resolution of 8 cm^{-1}.

Thermal Analysis. TG investigations were performed on a Netzsch STA 409 instrument, coupled with a Balzers QMG420/QMA125 quadrupole mass spectrometer and equipped with Pt−Rh thermocouples. A heating rate of 10 K min^{-1} and an air flow of 25 mL min^{-1} were used. Temperature-programmed reduction (TPR) was carried out with 20% H_2 in Ar by volume STP flowing at 25 mL min^{-1} and a heating rate of again 10 K min^{-1}.

Total carbon and hydrogen contents were determined with a LECO CHN-900 elemental microanalysis apparatus.

UV−Vis Diffuse Reflectance spectroscopy. Diffuse reflectance spectra were recorded on a Perkin-Elmer Lambda 16 spectrophotometer equipped with a 76 mm integrating sphere. $BaSO_4$ was used as reference. Prior to measurement, the samples were pretreated for 1 h at 410 K and 125 mbar, sealed, and cooled to ambient temperature. The reflectance spectra were digitalized and converted in the Kubelka−Munk function, which is proportional to the absorption coefficient.

^{51}V NMR Spectroscopy. The magic angle spinning ^{51}V NMR measurements were excited using a high-resolution solid mass NMR apparatus, Model Bruker AMX 400. The measurements were recorded at 105 MHz; the revolution speed of the 4 mm glass test tubes was 15 kHz. The isotropic chemical shift was determined with pure V_2O_5 (Fluka, purum) and amounted to −610 ppm. $VOCl_3$ was used as reference (∂ = 0 ppm). The experimental parameters used were taken from ref 41.

Results

Textural and chemical properties of the aerogels, both raw and calcined in air at different temperatures, are listed in Table 2.

Nitrogen Physisorption. In general, the aerogels showed a type-IV isotherm with a type-H2 desorption hysteresis according to IUPAC-classification[42] and mesoporosity with graphically determined maxima of the pore size distributions in the range 8−32 nm (Table 2). The adsorption/desorption isotherms, pore size distribution, and *t*-plot analysis of a portion of the low-temperature aerogel 5V*LT* calcined at 673 K are representatively depicted in Figure 1.

With regard to aging, it emerges from Table 2 that the BET surface areas of 5V*LT*a, both uncalcined and calcined in air at 673 K, were higher than those of the corresponding samples prepared without additional aging (5V*LT*); after calcination at 873 K they were virtually identical. However, the nitrogen pore volumes, mean pore sizes, and graphically determined maxima of the pore size distributions of the aged 5V*LT*a series gave all rise to about 2 times higher values compared to the samples of 5V*LT* whether raw or calcined in air up to 873 K.

An increase of the V content generally caused a significant decline in the microporosity, S_t, and BET surface area, S_{BET} (Table 2). After calcination at 673 K, the specific micropore surface areas, S_t, estimated from *t*-plot analysis, dropped from 167 to 39 $m^2\ g^{-1}$; the BET surface areas from 981 to 432 $m^2\ g^{-1}$. Up to 20 wt % nominal V_2O_5, the specific pore volumes, $V_{p(N_2)}$, lay in the range 1.4−1.9 $cm^3\ g^{-1}$; whereas for 30V*LT* with 30 wt % nominal V_2O_5 $V_{p(N_2)}$ decreased to 0.7 $cm^3\ g^{-1}$. With the corresponding sample of 5V*LT*−30V*LT*, similar tendencies became apparent after calcination at 873 K. Only 0V*LT* possessed smaller S_{BET} and S_t than 5V*LT* (Table 2).

The influence of the calcination temperature is reflected by the 5V*LT*, 5V*LT*a, and 20V*LT* series (Table 2). Note that a rise in temperature to 673 K caused an increase of S_{BET} from 705 to 888 $m^2\ g^{-1}$ and from 922 to 1108 $m^2\ g^{-1}$ for the samples of 5V*LT* and 5V*LT*a, respectively. However, at higher temperatures a significant decline in the BET surface areas was observed with all investigated aerogel samples except for the

(41) Fernandez, C.; Bodart, P.; Guelton, M.; Rigole, M.; Lefebvre, F. *Catal. Today* **1994**, *20*, 77.
(42) Sing, K. S. W.; Everett, D. H.; Haul, R. A. W.; Moscou, L.; Pierotti, R. A.; Rouquérol, J.; Siemieniewska, T. *Pure Appl. Chem.* **1985**, *57*, 603.

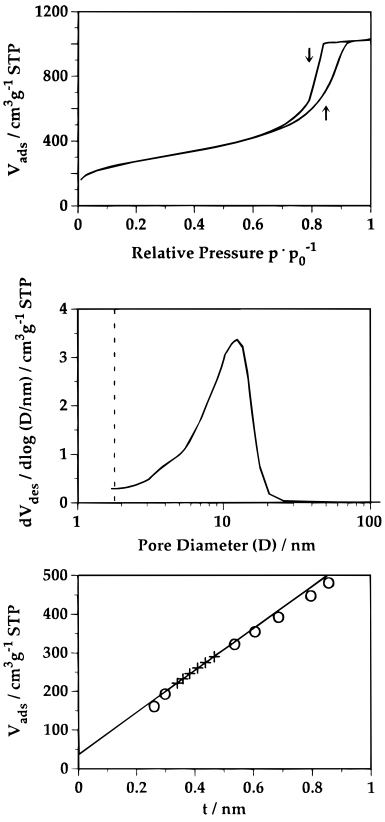

Figure 1. Nitrogen physisorption at 77 K on aerogel 5V*LT* calcined in air at 673 K. (a) adsorption (↑)/desorption (↓) isotherms (STP; 273.15 K, 1 atm); (b) pore size distribution derived from the desorption branch of nitrogen physisorption; (c) *t*-plot analysis (+ points taken for linear regression). Designations of samples are explained in the Experimental Section.

aerogel 5V*LT*. Calcination of a portion of 20V*LT* at 1173 K caused a drastic decrease in both S_{BET} and $V_{p(N_2)}$, accompanied by segregation−crystallization of V_2O_5 (see X-ray diffraction analysis).

X-ray Diffraction. X-ray diffraction analysis revealed that the 0V*LT*, 5V*LT*, 5V*LT*a, 10V*LT*, and 20V*LT* series were X-ray amorphous after calcination at temperatures ≤ 873 K and showed only a broad maximum characteristic for amorphous solids. The sample of 20V*LT*, calcined at 1073 K, however, contained crystalline V_2O_5.[43] In contrast, the 30V*LT* series with 30 wt % nominal V_2O_5, both raw and calcined in air up to 873 K, gave rise to distinct XRD patterns—besides the broad diffraction of the amorphous silica matrix (Figure 2). With the calcined samples, the reflection were assigned to crystalline V_2O_5,[43] whereas for the uncalcined aerogel an unidentified phase or compound had formed, which merits further investigation. A possible explanation might be the development of a vanadium oxohydroxy phase.

FTIR Spectroscopy. As an estimate for the frequency of Si−O−V entities in the mixed oxide, the ratio of the deconvoluted peak areas (*S*(Si−O−V)/*S*(Si−O−Si)) and its normalized *D*(Si−O−V) value, defined in eq

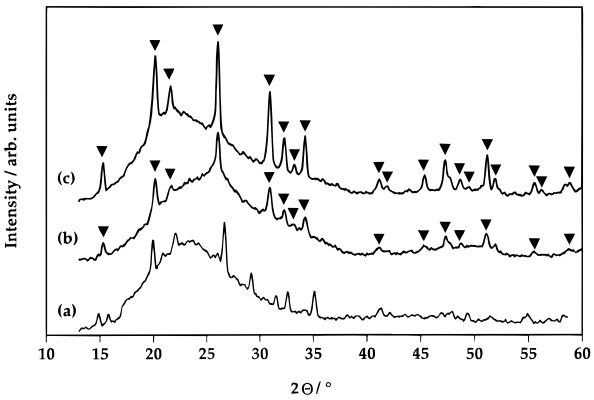

Figure 2. X-ray diffraction patterns (Cu Kα) of the 30V*LT* aerogel series: (a) raw, (b) calcined at 673 K and (c) calcined at 873 K. Designations of samples are explained in the Experimental Section. (▼) Vanadium pentoxide.

Table 3. Influence of Composition and Aging on Si−O−V Connectivity[a]

sample	*S*(Si−O−V)/*S*(Si−O−Si)[b]	*D*(Si−O−V)[c]
0V*LT*	0.00	0.00
5V*LT*	0.06	1.8
5V*LT*a	0.06	1.8
10V*LT*	0.11	1.5
20V*LT*	**0.23**	1.4
30V*LT*	0.15	0.5

[a] Designations of the samples are explained in the Experimental Section. [b] Relative contribution of Si−O−V entities, estimated from the ratio of Si−O−V (930−939 cm^{-1}) and Si−O−Si (1205−1215 cm^{-1}) peak areas. [c] *D*(Si−O−V); estimate of V dispersion derived from eq 1.

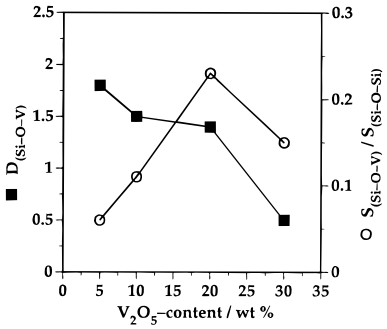

Figure 3. Influence of the V content on both the contribution of Si−O−V species estimated from the ratio *S*(Si−O−Ti)/*S*(Si−O−Si) (○) and the normalized Si−O−V connectivity (■) [*D*(Si−O−V), defined in eq 1], derived from FTIR analysis of the aerogels 5V*LT*, 10V*LT*, 20V*LT*, and 30V*LT* calcined in air at 873 K. *S*(Si−O−V) and *S*(Si−O−Si) are the peak areas of the Si−O−V band at 928−937 cm^{-1} and Si−O−Si band at 1206−1220 cm^{-1}, respectively. Designations of samples and analysis procedure are explained in the Experimental Section.

1, were quoted (Table 3). The ratio *S*(Si−O−V)/*S*(Si−O−Si) expresses an estimate of the total contribution of Si−O−V species, and *D*(Si−O−V) is supposed to represent a relative measure of the proportion of Si−O−V species referred to the overall molar V content and thus provides a kind of mixing efficiency, a quantity related to V dispersion (see Experimental Section).

For the aerogels 5V*LT*−30V*LT* calcined in air at 873 K, the influence of the content of nominal V_2O_5 in Si−O−V connectivity is illustrated in Figure 3.

An increase of the V content from 5 to 20 wt % "V_2O_5" caused a slight decline in *D*(Si−O−V), but prominent rise in *S*(Si−O−V)/*S*(Si−O−Si). As concerns 30V*LT* calcined at 873 K, both *D*(Si−O−V) and *S*(Si−O−V)/

(43) International Centre for Diffraction Data, File 9-0387, Newtown Square, PA.
(44) Scharf, U.; Schraml-Marth, M.; Wokaun, A.; Baiker, A. *J. Chem. Soc., Faraday Trans.* **1991**, *87*, 3299.
(45) Sanchez, C.; Livage, J.; Lucazeau, G. *J. Raman Spectrosc.* **1982**, *12*, 68.

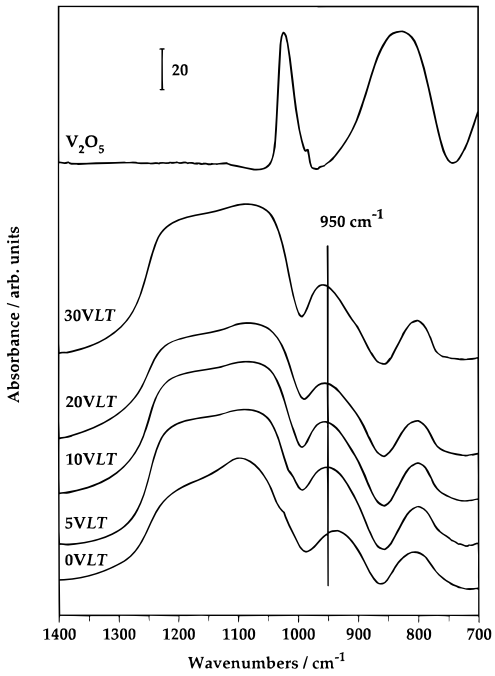

Figure 4. FTIR spectra of the dehydrated aerogels 0V*LT*, 5V*LT*, 10V*LT*, 20V*LT*, as well as 30V*LT* and unitary V_2O_5 (Fluka; purum). The aerogel samples were calcined in air at 873 K.

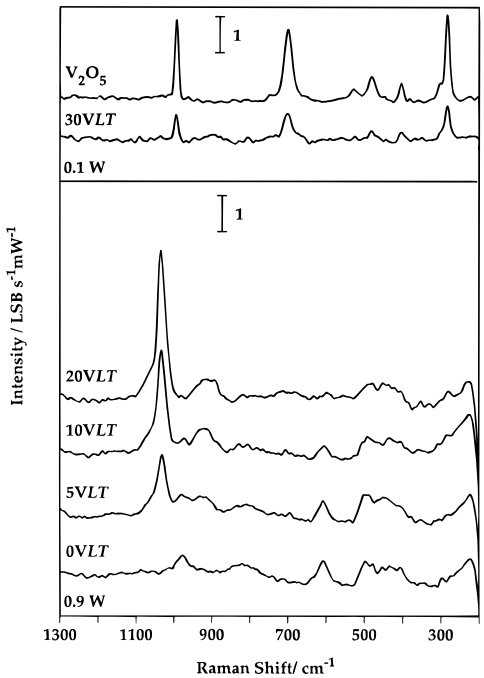

Figure 5. Raman spectra of the dehydrated aerogels 0V*LT*, 5V*LT*, 10V*LT*, 20V*LT*, as well as 30V*LT*, and unitary V_2O_5 (Fluka; purum). All aerogel samples were calcined in air at 873 K. Note that for samples V_2O_5 and 30V*LT* the laser power used was 0.1 W, whereas for all other samples 0.9 W were used. Designations of samples are explained in the Experimental Section.

S(Si−O−Si) drop to significantly lower values, which is in agreement with the segregation−crystallization of V_2O_5 (Figure 2). With regards to aging, 5V*LT* and 5V*LT*a, additionally aged for 16 days, gave rise to identical *D*(Si−O−V) and *S*(Si−O−V)/*S*(Si−O−Si) values. This behavior demonstrates that aging did not affect Si−O−V connectivity estimated from FTIR analysis.

FTIR spectra of the aerogels 0V*LT*, 5V*LT*, 5V*LT*a, 10V*LT*, 20V*LT*, as well as 30V*LT*, and unitary V_2O_5 (Fluka, purum) are shown in Figure 4. All samples exhibited typical bands at ca. 950 cm^{-1}. In the case of 0V*LT*, this band was assigned to Si−OH. As to the binary vanadia−silica aerogels, the relative intensity of this band compared to the bands at 800 and 1100 cm^{-1}, was distinctly higher. To suppress any deterioration of the Si−O−V analysis, the contribution of Si−OH was not taken into account, as specified in the Experimental Section.

Raman Spectroscopy. The influence of the vanadia loading on structure at molecular scale also arises from the Raman spectra depicted in Figure 5. A survey of the spectroscopic feature is listed in Table 4. In accordance with FTIR spectroscopy, the Raman spectra of 5V*LT* and 5V*LT*a, both calcined in air at 873 K, were virtually identical, indicative of comparable structural properties for both aerogel samples.

The unitary silica aerogel, 0V*LT*, calcined at 873 K showed bands at 400−450, 475−500, 610, 820 cm^{-1}, which are assigned to Si−O−Si vibrations. The band at 975 cm^{-1} stemmed from Si−OH vibration in dehydrated silica.[46] With the binary aerogels 5V*LT*, 10V*LT*, and 20V*LT*, all calcined at 873 K, the introduction of vanadia led to two additional bands—a prominent asymmetric V peak at 1030−1035 cm^{-1} and a minor one at ca. 920 cm^{-1}. The former is attributed to ν(V═O) vibration of tetrahedrally coordinated monomeric and oligomeric vanadyl species.[18,32] The latter originates from ν(V═O) of polyvanadate chains and ribbons with tetrahedral and square-pyramidal coordination.[17,44] The band at 975 cm^{-1} from Si−OH vibration[46] is assumed to be overlapped in the mixed systems by a band assigned to a basal plane V−O stretch,[32] corresponding to the band at 950−960 cm^{-1} in the FTIR spectra from Si−O−V stretching modes. At a loading of 20 wt % "V_2O_5", 20V*LT*, the silica vibrations were partially overlapped with a variety of stretching and deformational modes of small vanadia clusters. Thus, the observation of the weak, broad band at ca. 700 cm^{-1} is ascribed to the asymmetric O−V stretching mode of di- and trimeric vanadates. In addition the band at 285 cm^{-1} is assigned to the deformational motion δ(V═O) of multilayered VO_x, indicative of the presence of vanadia nanodomains. For 30V*LT* with 30 wt % "V_2O_5" and calcined at 873 K, this propensity for segregation−agglomeration finally resulted in the crystallization of V_2O_5, as corroborated by both the Raman features of V_2O_5 (Fluka) in Figure 5 and XRD (Figure 2).

Thermal Analysis. Thermal analysis was performed with 20V*LT* calcined at 873 K and a heating rate of 10 K min^{-1}. For the evolved gas analysis by mass spectroscopy, α-Al_2O_3 crucibles were used, which allowed larger amounts of sample and thus mass spectroscopy sensitivity compared to the Pt crucibles. The latter were applied for appropriate measurements of TG and especially DTA curves.

(46) Wood, D. L.; Rabinovich, E. M. *Appl. Spectrosc. C* **1989**, *43*, 263.
(47) Brinker, C. J.; Kirkpatrick, R. J.; Tallant, D. R.; Bunker, B. C.; Montez, B. *J. Non-Cryst. Solids* **1988**, *99*, 418.
(48) Bertoluzza, A.; Fagnano, C.; Morelli, M. A.; Gottardi, V.; Guglielmi, M. *J. Non-Cryst. Solids* **1982**, *48*, 117.

Table 4. Positions and Assignments of the Raman Bands for the Aerogel Samples Calcined in Air at 873 K[a]

0V*LT*	5V*LT*	5V*LT*a	10V*LT*	20V*LT*	30V*LT*	V_2O_5	assignment
	1030	1030	1030	1035			ν(V=O) of tetrahedrally coordinated monomeric and oligomeric species[18]
					995	993	ν(V=O) in multilayer structures, typical of crystalline V_2O_5[45]
975	980	975	980	980[w]			Si−OH in dehydrated silica[46] basal plane V−O stretch[32]
	920	920	920	920−890	900[w]		ν(V=O) of polyvanadate chains and ribbons with tetrahedral or square-pyramidal coordination[17,44]
820	810	800					Si−O−Si ring stretching vibration[19]
					700	700	crystalline V_2O_5[45]
610	605	605	605				breathing mode of cyclotrisiloxane[47]
					530[w]	530	crystalline V_2O_5[45]
					480[w]	480	crystalline V_2O_5[45]
500−475	500−480	500−475	490	485			breathing mode of cyclotrisiloxane[47]
450−400	450−400	440	450−400	460−400			Si−O−Si bending modes[48]
					403	403	crystalline V_2O_5[45]
				280[w]	300[wa]	300[wa]	crystalline V_2O_5[45]
					285	285	

[a] Designations of the samples are explained in the Experimental Section: [w]weak signal; [a]shoulder.

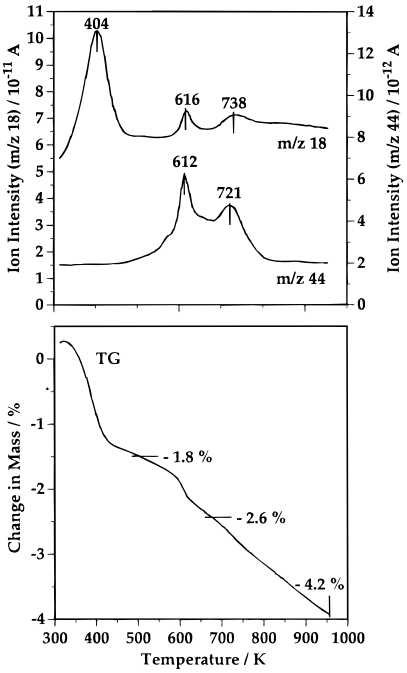

Figure 6. Thermoanalytical investigation on aerogel 20V*LT* calcined in air at 873 K. Bottom: TG curve. Top: ion intensities of $m/z(CO_2^+) = 44$ (CO_2) and $m/z(H_2O^+) = 18$ (H_2O). Heating rate 10 K min^{-1}; air flow 25 mL min^{-1}.

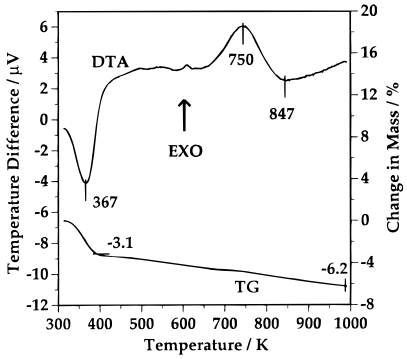

Figure 7. Thermoanalytical investigation on aerogel 20V*LT* calcined in air at 873 K. Bottom: TG curve. Top: DTA curve. Heating rate 10 K min^{-1}; air flow 25 mL min^{-1}.

The thermoanalytical results of 20V*LT* calcined at 873 K, measured in flowing air, are displayed in Figures 6 and 7.

The weight loss originated from the oxidation of organic residues and mainly from the evolution of water (desorption of physisorbed water, dehydroxylation), which was already present. This behavior arises from relating the TG curve to the monitored ion intensities of $m/z(CO_2^+) = 44$ and $m/z(H_2O^+) = 18$ (Figure 6). The H_2O evolution started at ambient temperature and reached a prominent maximum at 404 K followed by two minor peaks at 616 and 738 K. The H_2O liberation at the beginning originated from physisorbed water chiefly; at higher temperatures it was dominated by water from dehydroxylation and oxidation of the remnant organic residues. The CO_2 evolution began at ca. 450 K and attained maxima at 612 and 721 K. This behavior demonstrates that despite the calcination at 873 K for 5 h a considerable amount of organic residues persisted in the aerogels. These organic contaminants might be sitting deep inside the highly porous aerogel matrix. Their removal could thus be limited by diffusion. After cooling the above described sample to ambient temperature, a second thermoanalytical run was performed under identical conditions. The evolution of water was almost negligible, but surprisingly liberation of CO_2 could still be detected. The CO_2 evolutions of both runs resulted in a carbon content of 0.5−0.6 wt % for 20V*LT* calcined at 873 K, i.e., consistent with elemental microanalysis (Table 2).

The as-oxidized sample was then reduced in flowing H_2−Ar (20% H_2 by volume) by heating at 10 K min^{-1} to 1020 K—temperature-programmed reduction (TPR). The corresponding evolution of water reached its maximum at 824 K and was accompanied by a weight loss of 2.4 wt %. The integration of the peak areas for H_2O provided a content of nominal V_2O_5 of only 15 wt %. Independent analysis of the same sample by X-ray fluorescence spectroscopy (XRFS) analysis, however, confirmed the nominal content of 20 wt % "V_2O_5" for 20VLT. Consequently, the vanadia component was not fully either oxidized during the oxidative run or reduced in the TPR run.

The thermoanalytical run was repeated with less sample in a Pt crucible (Figure 7). In agreement with the above described results, the DTA curve in Figure 7 exhibits an endothermal signal at 367 K, related to the desorption of physisorbed water. The broad DTA signal at 750 K corresponds to the CO_2 evolution (Figure 6). Although the thermoanalytical run was stopped only at 1000 K, neither exothermal crystallization nor endothermal melting could be discerned, as subsequently confirmed by XRD.

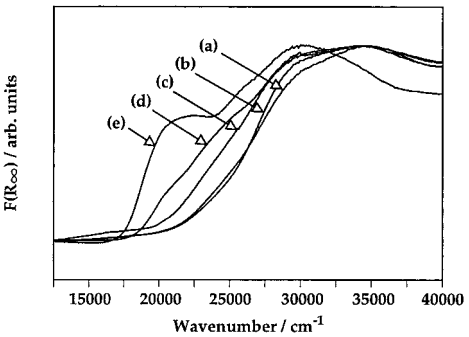

Figure 8. UV−vis diffuse reflectance spectra of dehydrated aerogels: (a) 5V*LT*, (b) 10V*LT*, (c) 20V*LT*, (d) 30V*LT*, and (e) V_2O_5 (Fluka; purum). All aerogel samples were calcined in air at 873 K. Designations of samples are explained in the Experimental Section.

All aerogels contained remarkable carbon contents, as deduced from elemental microanalysis (Table 2). These organic residues are likely to originate from realkoxylation of surface hydroxyl groups, incorporation of unhydrolyzed alkoxide ligands, and residual solvent in the SSG matrix.[22] A rise in the vanadia content from 0 to 20 wt % "V_2O_5" led to a distinct decline in residual carbon contents from 10.3 to 3.0 wt %. The uncalcined sample 30V*LT*, however, possessed 21.5 wt % carbon. It emerges from all series that only calcination at temperatures up to 873 K reduced the amount of organic contaminants to ≤0.2 wt % carbon (Table 2).

UV−Vis Diffuse Reflectance Spectroscopy. In general, the UV−vis spectra of vanadium ions are characterized by the lower-energy charge transfers (CT) in the range 20 000−29 000 cm^{-1} associated with O to V(V) electron transfers. The former region is ascribed to octahedral and square-pyramidal coordination, the latter range to tetrahedrally coordinated V(V) species. The CT transition for V(IV) occurs in the range 35 000−40 000 cm^{-1} and overlaps with the absorption of silica. The d−d transitions of VO^{2+} ions arise at ca. 13 000 and 16 000−18 000 cm^{-1}. Their appropriate intensities are generally 10−30 times lower than those of CT transitions.

The UV−vis spectra of 5V*LT*−30V*LT*, all calcined in air at 873 K, together with V_2O_5 reference are represented in Figure 8. All aerogel samples showed a broad absorption at ca. 34 000 cm^{-1} with a preceding shoulder at ca. 30 000 cm^{-1}, altogether representative of tetrahedrally coordinated VO^{3+} species. A rise in vanadia loading caused an increase in the absorption range 18 000−29 000 cm^{-1}, typical of octahedral V(V) coordination. This increase was especially evident for 20V*LT* and 30V*LT*, both calcined in air at 873 K. Moreover, with 30V*LT* two more shoulders would be discerned ca. 21 000 and 25 000 cm^{-1}, indicative of crystalline V_2O_5. In summary all the above UV−vis findings are again fully in agreement with XRD and vibrational spectroscopy.

The spectroscopic investigation of the 30V*LT* series is shown in Figure 9. The uncalcined parent aerogel exhibited a broad absorption in the range 14 000−24 000 cm^{-1}, possibly based on the absorption of VO^{2+} species, octahedrally coordinated V(V), and/or carbonaceous deposits. This absorption wavenumbers declined with calcination at 673 K. Finally, calcination at 873 K led to an increased absorption between 18 000 and 29 000 cm^{-1}, ascribed to octahedrally coordinated V(V) species and crystalline V_2O_5.

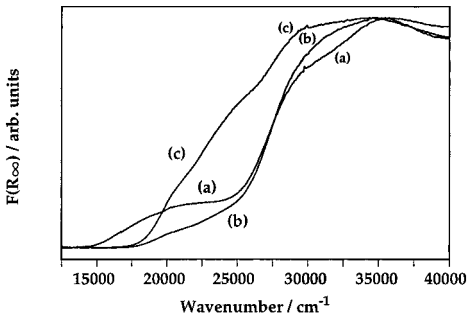

Figure 9. UV−vis diffuse reflectance spectra of the dehydrated 30V*LT* aerogel series: (a) uncalcined, (b) calcined in air at 673 K, and (c) calcined at 873 K.

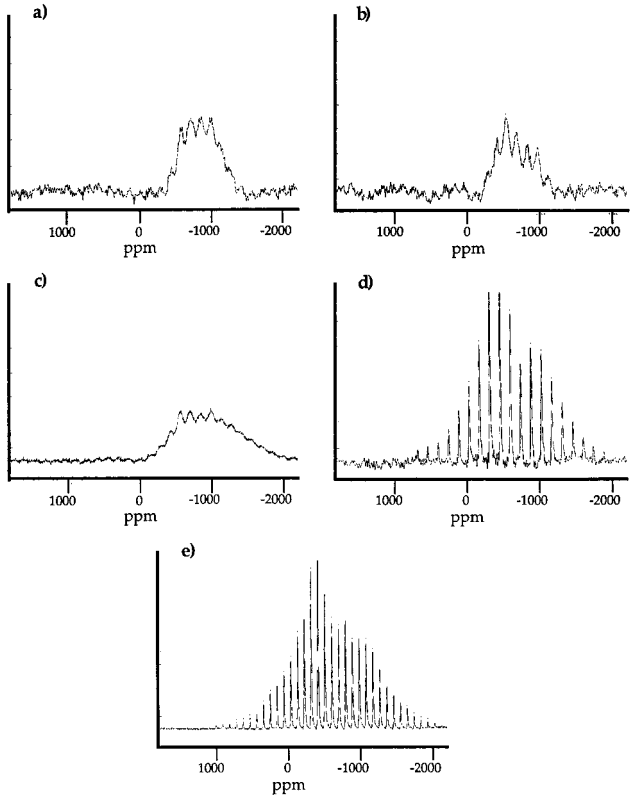

Figure 10. ^{51}V NMR investigation of the aerogels 5V*LT*, 10V*LT*, 20V*LT*, as well as 30V*LT*, and V_2O_5 (Fluka; purum). The aerogels were calcined in air at 873 K. Designations of samples are explained in the Experimental Section.

MAS ^{51}V NMR. The effect of vanadia loading on MAS ^{51}V NMR spectra is shown in Figure 10. The aerogel samples were all calcined in air at 873 K. An increase of the V_2O_5 content from 5 to 20 wt % led to a rise in low-field absorption, which is mirrored in the low-field shift of the absorption onset from −400 to −100 and −50 ppm for 5V*LT*, 10V*LT*, and 20V*LT*, respectively. This shift to low-field absorption is highly diagnostic of octahedral V^V.[49] The spectrum of 30V*LT* was in full agreement with the crystalline V_2O_5 quoted for comparison. The low-field absorption of both arose at about 650 ppm. These preliminary NMR studies merit further investigation in order to be able to make firm assignments, especially as concerns 5V*LT*, 10V*LT*, and 20V*LT* with pronounced V dispersion.

(49) Eckert, H.; Wachs, I. *J. Phys. Chem.* **1989**, *93*, 6796.

Studies on Stability for Liquid-Phase Catalysis. Recently, Neumann et al.[9] reported on the preparation of vanadia−silica xerogels with 7.4 wt % "V_2O_5" that were suggested to be stable and promising catalysts for liquid-phase oxidations with hydrogen peroxide. Accordingly to the procedure described in ref 9 such a xerogel was reproduced and quoted for comparison.

Studies on the liquid-phase oxidation of 1-phenylethanol in acetone−water with *tert*-butyl hydroperoxide resulted in higher activity for the aerogel catalysts. However, after microfiltration of the heterogeneous catalyst with 0.25 μm Teflon filters, a significant "quasi-homogeneous" contribution was detected for both the xerogel and the aerogel catalyst. This behavior demonstrates that both mixed oxides were not resistant toward the conditions applied. To poststabilize the aerogel catalysts, different pretreatments were examined, such as refluxing in methanol, water, water−H_2O_2, or water−HNO_3, but all attempts failed. Recalling the excellent thermal stability in air up to 873 K prompted us to investigate the catalytic performance in the gas phase. Preliminary results disclosed promising activity and selectivity in the partial oxidation of alkenes with air. Similarly, vanadia immobilized on different supports, V-substituted $ALPO_4$-5 zeolite,[50] and pure V_2O_5[51] suffered from lack of stability in peroxide-containing liquid media.

Discussion

Thermally stable, highly dispersed, and mesoporous vanadia−silica aerogels have been successfully prepared by an acid-catalyzed sol−gel route involving prehydrolysis and subsequent "gentle" removal of the solvent by semicontinuous extraction with supercritical CO_2 at 313 K. As to the sol−gel chemistry of vanadium alkoxides, Nabavi et al.[52] investigated hydrolysis and polycondensation of different alkoxides in dependence on hydrolysis level, n_{H_2O}:$n_{alkoxide}$. The authors demonstrated that the nature of the resulting materials varied significantly. Hydrolysis levels smaller than the stochiometric amount led to the formation of polymeric oxoalkoxy species. Such xerogels were generally X-ray amorphous after drying at ambient conditions. An aqueous gel was obtained by a large water excess, leading to a layered structure similar to V_2O_5 prepared by aqueous polycondensation of vanadic acid. Hirashima et al.[53] systematically studied the effects of hydrolysis level, alkoxide concentration, type of alkoxide, and pH and thus identified the regions in which sols, precipitates, or monolithic gels are formed. In conclusion, the sol−gel conditions chosen for our work (hydrolysis level of 2, acid:alkoxide ratio of 0.01, alkoxide concentration in the range 11.3−11.45 mol %) are likely to account for the formation of small vanadia species. These conditions in conjunction with acid catalysis and prehydrolysis, which "decouples" hydrolysis and condensation of VOTIP and confers a margin on the less reactive TEOS, respectively, lend themselves to yield high Si−O−V connectivity and thus V dispersion. Addition of acid accelerated hydrolysis and decelerated condensation, resulting in an increase of gelation time. Upon modification of the alkoxide ligands, the hydrolysis rate decreased in the order ethoxide > butoxide > isopropoxide. The latter two aspects are common properties of many other metal alkoxide system.[19,27]

Influence of Aging. The aging of an SSG sample is a useful dynamic means consolidating the wet-chemical structure by continuous condensation, esterification, dissolution, reprecipitation, depolymerization, and repolymerization. The processes in operation include Ostwald ripening, coalescence-coarsening, sintering, and syneresis.[22] The latter process reflects spontaneous shrinkage and thus network densification by continuous condensation reactions or attraction between agglomerates. Aging is generally a function of time, temperature, and pH and nature of the aging fluid.[54]

The textural properties of the aerogels 5V*LT* and 5V*LT*a possess a marked dependence on the aging procedure chosen. With aging at basic pH for 16 days, the BET surface area, mesoporosity, and pore volume increased, whereas the contribution of microporosity decreased (Table 2). In the case of titania−silica xerogels, Handy et al.[39] found a similar behavior when aging resuspended aerogels in basic medium. Another aspect of aging is the concomitant increase in gel rigidity, which is crucial in order to withstand drying stresses. Rangarajan and Lira[55] observed that in the case of repetitive purging with liquid CO_2 at 291 K and 5.5 MPa followed by SCD at 313 K, shrinkage of silica gels, mainly due to syneresis, primarily occurred during depressurization at the end of SCD. They assigned this shrinkage to stresses within the gel network due to adsorption phenomena and demonstrated that aging of the gels prior to SCD reduced the impact of shrinkage. In essence, aging significantly affects the resultant textural properties, whereas composition and structure of the vanadia component remain virtually unaffected.

Influence of the Vanadia Content. An increase of the V content from 5 to 30 wt % nominal V_2O_5 led to a decline in both BET surface area and microporosity (Table 2). The marked mesoporosity of these samples, combined with their high thermal stability up to 873 K, renders these aerogels promising candidates for use in gas-phase catalysis. Note that the wide pores make the large internal surface area accessible for bulky reactants.

The dependence of the rise in V content on the textural properties might stem from the increasing amount of base used in order to force gelation (see Experimental Section). At a pH of >ca. 10, SiO_2 begins to dissolve,[56] enhancing Ostwald ripening, coalescence−coarsening, and syneresis. These processes often lead to a decrease in BET surface area and microporosity as well as a concomitant rise in mesoporosity.

The investigation of the Si−O−V connectivity yields the highest D(Si−O−V) value for the aerogel 5V*LT* with 5 wt % "V_2O_5" (Table 3, Figure 3). Upon increase to 20 wt % "V_2O_5", the D(Si−O−V) values decrease gradually, whereas the contribution of ν(Si−O−V) vibrations,

(50) Whittington, B. I.; Anderson, J. R. *J. Phys. Chem.* **1993**, *97*, 1032.
(51) Sheldon, R. A. *Aspects of Homogeneous Catalysis*; Ugo, R., Ed.; Reidel: Dordrecht, 1981; p 3.
(52) Nabavi, M.; Sanchez, C.; Livage, J. *Eur. J. Solid State Inorg. Chem.* **1991**, *28*, 1173.
(53) Hirashima, H.; Tsukimi, K.; Muratake, R. *J. Ceram. Soc. Jpn. Int. Ed.* **1989**, *97*, 232.
(54) Smith, D. M.; Davis, P. J.; Brinker, C. J. *Mater. Res. Soc. Symp. Proc.* **1990**, *180*, 235.
(55) Rangarajan, B.; Lira, C. T. *J. Supercrit. Fluids* **1991**, *4*, 1.
(56) Iler, R. K. *The Chemistry of Silica*; John Wiley: New York, 1979.

expressed as S(Si−O−V)/S(Si−O−Si), increases distinctly and attains a maximum. In the case of 30 wt % "V_2O_5", however, both D(Si−O−V) and the ratio S(Si−O−V)/S(Si−O−Si) decline essentially. This behavior shows that a rise in V content accounts for the increased formation of V−O−V structural units, which even grow to crystalline V_2O_5, as independently corroborated by XRD (Figure 2), Raman spectroscopy (Figure 5), UV−vis spectroscopy (Figures 8 and 9), and ^{51}V NMR (Figure 10). Consequently, the limit for high "mixing efficiency" seems to be at ca. 20 wt % "V_2O_5" (20VLT).

In essence, the use of S(Si−O−V)/S(Si−O−Si) and D(Si−O−V) values as estimates of Si−O−V connectivity seems to represent a useful means to characterize the vanadium dispersion. For titania−silica, we have demonstrated that these estimates of heteroconnectivity are correlated with the catalytic activity in epoxidation of bulky olefins.[1,2]

Effects of the Calcination Temperature. The increase in BET surface area during calcination in air at 673 K resides in the removal of organic residues, rendering the surface accessible for the physisorption of nitrogen[57] (Table 2). The subsequent decrease at temperatures > 673 K is likely to originate from processes such as Ostwald ripening, coalescence−coarsening, sintering, and syneresis.

As concerns the thermal stability of the V dispersion, the appropriate estimates for Si−O−V connectivity are virtually unaffected by the calcination temperatures ≤ 873 K. Only calcination at 1173 K induced segregation−crystallization of V_2O_5. Moreover, it emerged from thermal analysis that a sample of 20VLT, which had been two times oxidatively treated at 1000 K, contained only 15 wt % reducible "V_2O_5". A similar behavior was observed for vanadia−silica xerogels prepared from a mixture of vanadia and silica hydrosols[8] and xerogels with low V/Si ratios (0.005−0.5%) prepared by hydrolysis of alkoxides in alcoholic solvent.[10] In addition, spectroscopic studies disclosed that the vanadium ions are surrounded by oxygen ions, all being in bridging positions in an amorphous oxidic network.[58]

(57) Yamane, M.; Aso, S.; Okano, S.; Sakaino, T. *J. Mater. Sci.* **1979**, *14*, 607.

Conclusions

Mesoporous and highly dispersed vanadia−silica aerogels have been prepared via an acid-catalyzed sol−gel route including prehydrolysis and subsequent "gentle" removal of the solvent by semicontinuous extraction with supercritical CO_2. Acid catalysis in conjunction with prehydrolysis, which "decouples" hydrolysis and condensation, and matching precursor reactivities, lend themselves to yield highly dispersed vanadia−silica mixed oxides. Spectroscopy (FTIR, Raman, UV−vis, ^{51}V NMR) proved to represent a salient means for the characterization of structure and composition at molecular scale. As concerns FTIR, the importance of the band due to ν(Si−O−V) at ca. 940−960 cm^{-1} became evident and its ratio to the band at ca. 1210 cm^{-1} due to ν(Si−O−Si) led to useful estimates of the vanadium dispersion. An increase of the vanadia content from 5 to 20 wt % nominal V_2O_5 caused a gradual decline in vanadium dispersion, whereas the absolute contribution of Si−O−V connectivity increased. For 30 wt % "V_2O_5", both measures decrease essentially and the continuous formation of V−O−V connectivity results in segregation−crystallization of V_2O_5. The effect of aging in basic medium confines to the textural properties, significantly increasing BET surface area and especially pore volume. Possible processes in operation are Ostwald ripening, coalescence coarsening, and syneresis. With regard to the catalytic application, the severe lack of stability in protic solvents and aprotic media in conjunction with peroxides is superseded by the high thermal stability in air at ≤873 K, which renders the vanadia−silica aerogels interesting for catalytic oxidation in the gas phase.

Acknowledgment. Thanks are due Marek Maciejewski and Felix Bangerter for performing thermal analysis and NMR spectroscopy. Financial support by the Swiss National Science Foundation (2129-041850.94) is kindly acknowledged.

CM9504293

(58) Wokaun, A.; Schraml, M.; Baiker, A. *J. Catal.* **1989**, *116*, 595.